WILEY-VCH

Yanpeng Zhang, Feng Wen, and Min Xiao

Quantum Control of Multi-Wave Mixing

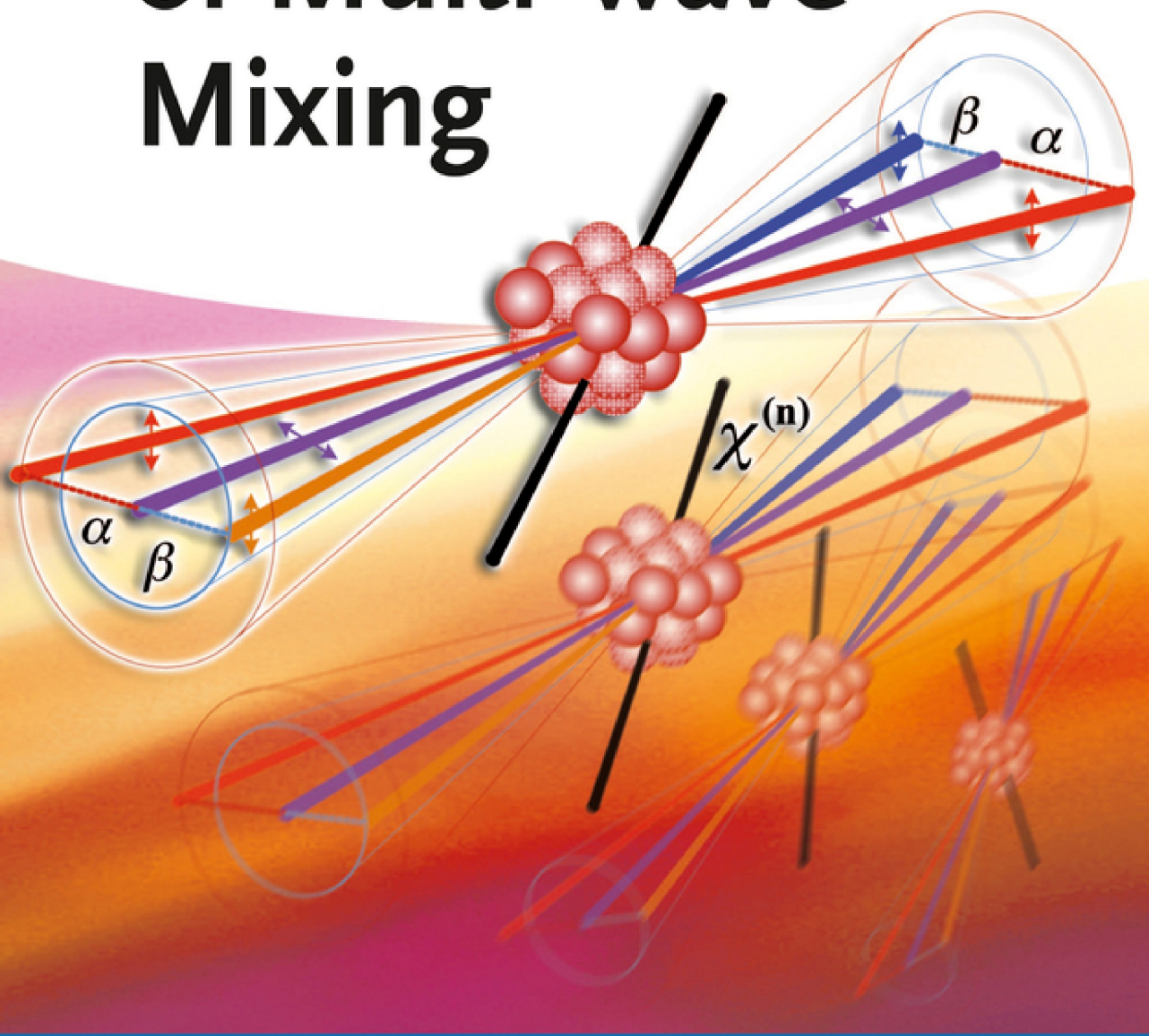

高等教育出版社
HIGHER EDUCATION PRESS

Yanpeng Zhang, Feng Wen, and Min Xiao

Quantum Control of Multi-Wave Mixing

Related Titles

Prather, D.W., Shi, S., Sharkawy, A., Murakowski, J., Schneider, G.

Photonic Crystals

Theory, Applications and Fabrication

2009
ISBN: 978-0-470-27803-1

Ishikawa, H.

Ultrafast All-Optical Signal Processing Devices

2008
ISBN: 978-0-470-75869-4

Saleh, B.E., Teich, M.C.

Fundamentals of Photonics, Second Edition

2nd Edition

2007
ISBN: 978-0-471-35832-9

Stegeman, G.I., Stegeman, R.F.

Nonlinear Optics

Phenomena, Materials, and Devices

2012
ISBN: 978-1-118-07272-1

Mandel, P.

Nonlinear Optics

An Analytical Approach

2010
ISBN: 978-3-527-40923-5

Chen, C., Sasaki, T., Li, R., Wu, Y., Lin, Z., Mori, Y., Hu, Z., Wang, J., Yoshimura, M., Kaneda, Y.

Nonlinear Optical Borate Crystals

Principles and Applications

2012
Print ISBN: 978-3-527-41009-5
Also available in digital formats.

Yanpeng Zhang, Feng Wen, and Min Xiao

Quantum Control of Multi-Wave Mixing

WILEY-VCH
Verlag GmbH & Co. KGaA

高等教育出版社
HIGHER EDUCATION PRESS

The Authors

Prof. Yanpeng Zhang
Xi'an Jiaotong University
Department of Electronics
No. 28, Xianning West Road
Department of Electronics
710049 Xi'an, Shaanxi
China
ypzhang@mail.xjtu.edu.cn

Dr. Feng Wen
Xi'an Jiaotong University
Department of Electronics
No.28, Xianning West Road
Department of Electronics
710049 Xi'an, Shaanxi
China

Prof. Min Xiao
University of Arkansas
Department of Physics
PHYS 204
Department of Physics
United States

Cover
Geometry of the preparation of the entangled photon source experiment. The pump in purple is focused on an atomic group and couples with probe and conjugate fields located symmetrically at a small angle in respect to the pump axis, then the generated FWM and SWM photons are entangled in the frequency and spatial space.

Additional book-related material for lecturers can be found online at www.wiley-vch.de and www.wiley.com.

Library of Congress Card No.: applied for

British Library Cataloguing-in-Publication Data
A catalogue record for this book is available from the British Library.

Bibliographic information published by the Deutsche Nationalbibliothek
The Deutsche Nationalbibliothek lists this publication in the Deutsche Nationalbibliografie; detailed bibliographic data are available on the Internet at <http://dnb.d-nb.de>.

Published by Wiley-VCH GmbH & Co.KGaA; Boschstr. 12, 69469 Weinheim, Germany, under exclusive license granted by Higher Education Press Limited Company for all media and languages excluding Chinese and throughout the world excluding Mainland China and with non-exclusive license versions in Mainland China.

Print ISBN: 978-3-527-41189-4
ePDF ISBN: 978-3-527-67239-4
ePub ISBN: 978-3-527-67238-7
mobi ISBN: 978-3-527-67237-0
oBook ISBN: 978-3-527-67236-3

Cover Design Adam-Design, Weinheim
Typesetting Laserwords Private Limited, Chennai, India
Printing and Binding Markono Print Media Pte Ltd, Singapore

Printed on acid-free paper

Contents

Preface

It is widely agreed that the optical properties of materials change drastically in systems where the superpositions of quantum states are coherently excited. Many interesting scientific discoveries and technical applications have been made with nonlinear optical effects in several kinds of nonlinear materials. Examples of such effects include the modification of absorptive properties resulting in electromagnetically induced transparency (EIT) and lasing without population inversion, as well as the modification of dispersive properties to give a resonantly enhanced index of refraction accompanied by vanishing absorption. There are already several excellent general textbooks covering various aspects of nonlinear optics, including ''*Nonlinear Optics*'' by R. W. Boyd, ''*Nonlinear Optics*'' by Y. R. Shen, ''*Quantum Electronics*'' by A. Yariv, ''*Nonlinear Fiber Optics*'' by G. P. Agrawal, ''*Photons and Nonlinear Optics*'' by D. N. Klyshko, and so on. Although these textbooks have provided solid foundations for readers to understand various nonlinear optical processes, some comprehensive and deep knowledge on a certain nonlinear optical effect is essential for studying and researching. With the intention of giving the special knowledge and recent progress about multi-wave mixing (MWM) effect, the authors have published two earlier monographs, ''Multi-Wave Mixing Processes'' and ''Coherent Control of Four-Wave Mixing'' in 2009 and 2011, respectively, which covers the experimental and theoretical studies of several topics related to MWM processes previously done in authors' groups. The topics covered in the two monographs include difference-frequency femtosecond and sum-frequency attosecond beats of four-wave mixing (FWM) processes; heterodyne detections of FWM, six-wave mixing (SWM), and eight-wave mixing (EWM) processes; the Raman, Raman–Rayleigh, Rayleigh–Brillouin, and coexisting Raman–Rayleigh–Brillouin-enhanced polarization beats; high-order correlation functions of different noisy fields on the femto- and attosecond polarization beats, and heterodyne/homodyne detections of the ultrafast third-order polarization beats.

This new monograph is built on the previous works and extends them significantly. The intention is to present all the additional and new works done in recent years in authors' groups. Also, many added latest results, extended detailed calculations, and more deep discussions are cited from the already published papers, which can help readers better appreciate the interesting nonlinear optical phenomena.

Besides showing more results on controls and interactions between MWM processes in hot atomic media, this monograph also presents and discusses several novel types of spatial solitons and two-photon fluorescence in the FWM process, which are completely new phenomena in multi-level atomic systems.

Chapter 1 gives the outline of this monograph and introduce some basic concepts frequently used in the later chapters, such as the suppression and enhancement conditions of MWM, two- and three-photon fluorescence, MWM in ring optical cavity, photonic band gap, and MWM with Rydberg blockade, and so on. Chapter 2 gives the extended results on the EIT-assisted MWM which includes not only the coexistence of FWM, SWM, and EWM signals in multi-EIT windows, but also the interplay and interference among the multiple MWM processes. Chapter 3 gives the results on the ac-Stark effect and Autler–Townes (AT) splitting in the MWM process, which can be accurately explained by multi-dressed state theory. Chapter 4 presents the switching methods between enhancement and suppression of MWM in both frequency and spatial domains, and the evolution of the dressed effects from pure enhancement into pure suppression when the probe detuning as well as the powers of the dressing and probe fields are changed. Chapter 5 shows the polarization-controlled MWM processes in multiple Zeeman sublevels system, in which the generated MWM signals can be modified and controlled, and the dark-state effects can be controlled to evolve from pure enhancement into pure suppression in the MWM processes via the polarization states of the laser beams. Chapter 6 presents the demonstration of the modification and control of the two-photon fluorescence process and three-photon correlation in MWM by manipulating the dark-state or EIT windows. On the other hand, the vacuum-induced Rabi splitting and optical bistability in a coupled atom-cavity system is also included. Chapter 7 shows the forming of electromagnetically induced grating (EIG) and electromagnetically induced lattice (EIL) in FWM, which can lead to spatial shift and splitting of laser beams as well as several novel types of spatial solitons of FWM signals, such as gap, dipole, vortex, and surface solitons with the generated FWM beams in different regions in experimental parametric space. Chapter 8 presents the observations of the prototype investigation of all-optical switches, routers, and space demultiplexer by the FWM process.

The authors believe that the current monograph treats some special topics of quantum controls of MWM and can be useful to researchers who are interested in the related fields. Several features presented here are distinctly different from and more advanced than the previously reported works. For example, the authors have shown the two-photon ac-Stark effect and AT splitting of MWM can be used to determine the energy-level shift of the atom. Also, theoretical calculations are in good agreement with the experimentally measured results in demonstrating the two phenomena in MWM processes. Efficient spatial–temporal interference between FWM and SWM signals generated in a four-level atomic system has been carefully investigated, which exhibits controllable interactions between two different (third- and fifth-) order nonlinear optical processes. Evolutions of the enhancement and suppression of MWM signals under various dressing schemes are experimentally investigated, and can be explained in detail with dressing state

theory. Such controllable high-order nonlinear optical processes can be used for designing new devices for all-optical communication and quantum information processing.

The authors also experimentally compare the intensity spectra of probe transmission, FWM, and fluorescence signals under dressing effects, in which the two-photon fluorescence signal with ultranarrow line width much less than the Doppler-free EIT window is obtained. Moreover, the three photons of the two coexisting FWM signals and the probe signal in a double-lambda-type system are experimentally found to be strongly correlated, or anticorrelated with each other. Such ultranarrow linewidth fluorescence, strongly correlated or anticorrelated photons and controllable cavity mode splitting as well as the optical bistability process could have potential applications in optical communication and quantum information processing.

The authors also experimentally demonstrate that by arranging the strong pump and coupling laser beams in specially designed spatial configurations (to satisfy phase-matching conditions for efficient MWM processes), the generated MWM signals can be spatially shifted and split controllably by the cross-phase modulation (XPM) in the Kerr nonlinear medium. Therefore, the periodic splitting of the metastable energy level and periodic refractive index of the medium is experimentally obtained by the spatially periodic interfered pattern of dressing fields. Moreover, in the propagation of FWM or probe beams, when the spatial diffraction is balanced by XPM, the spatial beam profiles of the beams can become stable to form spatial optical solitons. For different geometrical configuration and experimental parameters (such as laser powers, frequency detunings, and temperature), novel gap, vortex, dipole, and surface soliton have been shown to experimentally appear in the multi-level atomic system in vapor cells. These studies have opened the door for achieving all-optical controlled spatial switch, routing, and soliton communications with an ultrashort response time.

This monograph serves as a reference book intended for scientists, researchers, graduate students, and advanced undergraduates in nonlinear optics and related fields.

We take this opportunity to thank all the researchers and collaborators who have worked on the research projects as described in this book.

Yanpeng Zhang, *Feng Wen*, and *Min Xiao*

1
Introduction

The subjects of this book center mainly around three topics. The first topic (Chapters 2–5) covers the quantum interference of coexistent four-wave mixing (FWM) processes because the generated FWM signal can be selectively enhanced or suppressed via electromagnetically induced transparency (EIT) windows and induced atomic coherence. Both enhancement and suppression of dressed FWM can be observed directly by scanning the dressing field instead of the probe field. With specially designed spatial patterns and phase-matching conditions for laser beams, coexisting FWM and six-wave mixing (SWM) processes can also be generated very efficiently. Also, three dual-dressed schemes (nested, sequential, and parallel) of coexisting FWM have been studied. Frequency, spatial, and temporal interferences that occur between two different wave mixing processes for the relative phase between different multi-wave mixing (MWM) processes is modulated. In such cases, the FWM and SWM signals are modulated with phase difference. By regulating the laser beam, the constructive and destructive interference can be selected, and then ac-Stark effect and Autler–Townes (AT) splitting are observed. Furthermore, by manipulating the polarization states of the laser beams, the MWM processes can also be modified and controlled. The second topic (Chapter 6) relates to nonclassical properties of the MWM process; the correlation or anticorrelation between two coexisting FWM signals; and comparison among the depths of the probe transmission, FWM, and the two-photon fluorescence signals in the same nonlinear process. Especially, one can switch from bright to dark states in the FWM and fluorescence channels with the relative phase modulated from 0 to $-\pi$. The relationship of vacuum Rabi splitting (VRS) and optical bistability (OB) of cavity MWM signals and methods to control VRS and OB are also included. The third topic (Chapters 7 and 8) relates to the interplays in frequency and spatial domains of MWM processes induced by atomic coherence in multi-level atomic systems. The generated two-dimensional surface solitons, multi-component dipole, and vortex vector solitons of the MWM signal accompanying the formation of electromagnetically induced lattice (EIL) are presented in Chapter 7. Finally, an application of spatial displacements and splitting of the probe and generated FWM beams, that is, all-optical spatial routing, switching, and demultiplexer are shown and investigated in Chapter 8. Experimental results are presented and compared with the theoretical calculations

Quantum Control of Multi-Wave Mixing, First Edition. Yanpeng Zhang, Feng Wen, and Min Xiao.

throughout the book. In this book, the emphasis is on the work done by the authors' groups in the past few years. Some of the work presented in this book are built on our previous books ''Multi-wave Mixing Processes'' and ''Coherent Control of Four-Wave Mixing,'' published by Higher Education Press and Springer 2009 and 2011, respectively, where we have mainly discussed the coexistence and interactions between efficient MWM processes enhanced by atomic coherence in multi-level atomic systems in the former, and in the latter the control in frequency and spatial domains of FWM processes induced by atomic coherence in multi-level atomic systems. Before starting the main topics of this book, some basic physical concepts and mathematical techniques, which are useful and needed in the later chapters, are briefly introduced and discussed in this introduction chapter.

1.1
Suppression and Enhancement Conditions of the FWM Process

In this section, the dressed state theory with suppression and enhancement of FWM, dark-state theory in high-order nonlinear processes is introduced. Specifically, in Section 1.1.1, we discuss different dressing states including singly dressing and doubly dressing states. And the AT splitting for FWM by scanning the detuning of the probe field induced by the dressing effect will also be introduced. In Section 1.1.2, the same phenomenon is investigated using the quantum interference method. Also, we discuss that the high-order nonlinear processes can be effectively controlled by the dark state. In Section 1.1.3, we focus on suppression and enhancement of the FWM process by scanning the detuning of the dressing field. In addition, the interaction between dressing fields is introduced in different dressing schemes.

1.1.1
Dressed State Theory

The most successful applications of resonant systems is in the two-photon rather than single-photon transition process because EIT [1, 2] forming in a two-photon interference process can reduce the linear absorption of a probe beam with a strong coupling beam resonant with the up-level transition. For example, enhanced MWM processes due to two-photon Raman resonances [3, 4] have been experimentally demonstrated in several multi-level atomic systems [5–7]. The keys in such enhanced nonlinear optical processes include the enhanced nonlinear susceptibilities due to induced atomic coherence and slowed laser beam propagation in the atomic medium [8–10], as well as greatly reduced linear absorption of the generated optical fields due to EIT [11]. By changing the strength [12], detuning [13], polarization [7], and phase [14] of the dressing fields, the EIT window and nonlinear susceptibilities

can be effectively modulated. Therefore, the generated MWM signal can be enhanced or suppressed selectively. On the other hand, AT splitting of the MWM [15–17] signal can be controlled effectively at the same time.

In order to describe more precisely what is the physics meaning of the AT splitting and suppression or enhancement of the wave mixing process mentioned, we introduce the dressing state theory first and use it to briefly describe the relations between the AT splitting and the suppression or enhancement of MWM.

In Figure 1.1(a), the external dressing field $\boldsymbol{E}_3$ and self-dressing field $\boldsymbol{E}_2$ ($\boldsymbol{E}_2'$) dress the energy level $|1\rangle$ simultaneously. First, $\boldsymbol{E}_2$ ($\boldsymbol{E}_2'$) splits the state $|1\rangle$ to create the primary dressed states $|\pm\rangle$ written as $|\pm\rangle = \sin\theta_1|1\rangle + \cos\theta_1|2\rangle$. We can obtain the eigenvalues of $|+\rangle$ and $|-\rangle$ as $\lambda_+ = (\Delta_2 + \sqrt{\Delta_2^2 + 4|G_2|^2})/2$ and $\lambda_- = (\Delta_2 - \sqrt{\Delta_2^2 + 4|G_2|^2})/2$ (measured from level $|1\rangle$), respectively, as shown in Figure 1.1(b). Next, $\boldsymbol{E}_3$ further splits $|+\rangle$ or $|-\rangle$ to create the secondary dressed states $|+\pm\rangle$ or $|-\pm\rangle$ determined by the detuning of $\boldsymbol{E}_3$, as shown in Figure 1.1(c) and (d). For instance, if $\boldsymbol{E}_3$ couples with the upper dressed state $|+\rangle$, then secondary dressed states are given as $|+\pm\rangle = \sin\theta_2|+\rangle + \cos\theta_2|3\rangle$ (Figure 1.1(c)), where $\sin\theta_1 = -a_1/a_2$, $\cos\theta_1 = G_2^b/a_2$, $\sin\theta_2 = -a_3/a_4$, $\cos\theta_2 = G_3/a_4$, $a_1 = \Delta_2 - \lambda_\pm$, $a_2 = \sqrt{a_1^2 + |G_2^b|^2}$, $a_3 = \Delta_3 - \lambda_+ - \lambda_{+\pm}$, $a_4 = \sqrt{a_3^2 + |G_3|^2}$, and $G_2^b = G_2 + G_2'$. The eigenvalues of $|++\rangle$ and $|+-\rangle$ are $\lambda_{++} = (\Delta_3' + \sqrt{\Delta_3'^2 + 4|G_3|^2})/2$ and $\lambda_{+-} = (\Delta_3' - \sqrt{\Delta_3'^2 + 4|G_3|^2})/2$ (measured from level $|+\rangle$), respectively, where $\Delta_3' = \Delta_3 - \lambda_+$.

By scanning the detuning of the probe field (Δ_1), the primary AT splitting for the FWM signal (Figure 1.2(a)), or primary and secondary AT splitting (Figure 1.2(b)) can be obtained. In Figure 1.2(a), the AT splitting that results from the field $\boldsymbol{E}_2$ ($\boldsymbol{E}_2'$) has two bright states (two peaks) and one dark state (the dip at $\Delta_1 = 0$), and the splitting separation $\Delta_{\lambda 1}$ ($\Delta_{\lambda 1} = \lambda_+ - \lambda_-$) gets larger with the power of $\boldsymbol{E}_2$ ($\boldsymbol{E}_2'$) increasing. In addition, if $\boldsymbol{E}_3$ also couples $|-\rangle$, Figure 1.2(b) presents the primary and secondary AT splitting for different coupling field power P_3. It is obvious that the secondary AT splitting $\Delta_{\lambda 2}$ ($\Delta_{\lambda 2} = \lambda_{++} - \lambda_{+-}$) (Figure 1.2(b)) gets larger with increasing power of $\boldsymbol{E}_3$.

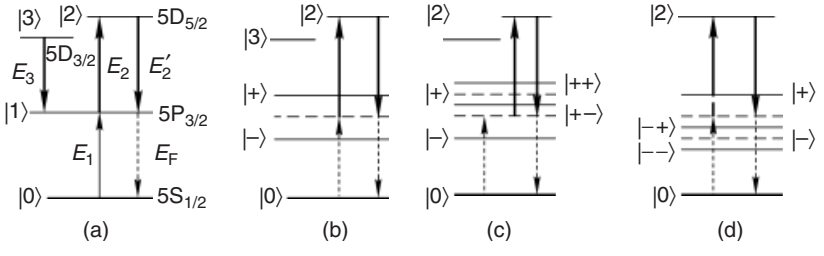

Figure 1.1 The diagrams of (a) a Y-type four-level, (b) the singly-dressed state, and (c) and (d) the doubly-dressed state.

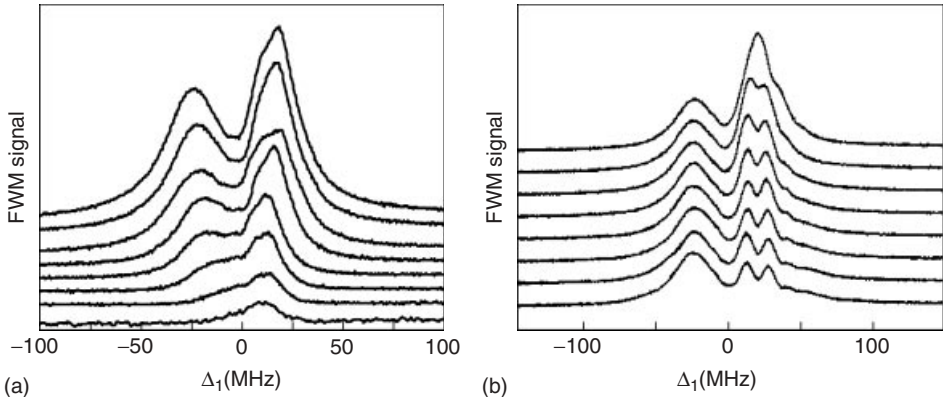

Figure 1.2 (a) Measured primary AT splitting and (b) primary and secondary AT splitting of FWM signals.

1.1.2 Dark-State Theory in MWM Processes

In the following, we discuss in detail the dark-state theory in three-level, Y-type four-level, and K-type five-level. The evolution of the FWM signal is fitted well with the theoretical calculation [5, 14].

Well known in quantum optics, the phenomenon of coherent dark states [18] is based on a superposition of long-lived system eigenstates that decouple from the light field. The dark state can be used to make a resonant, opaque medium transparent by means of quantum interference. Associated with the induced transparency is a dramatic modification of the refractive properties; therefore, it has found numerous applications. Prominent examples are EIT and lasing without inversion [19, 20], subrecoil laser cooling [21], and ultrasensitive magnetometers [22]. The possibility of coherently controlling the propagation of quantum light pulses via dark-state polaritons opens up interesting applications involving the generation of nonclassical states in atomic ensembles (squeezed or entangled states), reversible quantum memories for light waves [23–25], and high-resolution spectroscopy [26–28]. Furthermore, the combination of the present technique with studies on few-photon nonlinear optics [29–31] can be used, in principle, for processing of quantum information stored in collective excitations of matter. In the following, we discuss how high-order nonlinear processes can be effectively controlled by the dark state.

First, let us consider how a simple FWM process in a Ξ-type three-level could be manipulated and analyzed with the dark-state theory developed in this section. As shown in Figure 1.3, in the interaction picture, the Hamilton of a coupled atom-field system can be written as $H = \hbar(G_1|1\rangle\langle 0|\exp(-i\Delta_1 t/\hbar) + G_2|1\rangle\langle 2|\exp(-i\Delta_2 t/\hbar) + \mathrm{HC})$, and the wave function of an atom in bare state is $|\psi\rangle = c_0(t)|0\rangle + c_1(t)|1\rangle + c_2(t)|2\rangle$. If the coupled system of the laser field and atom is

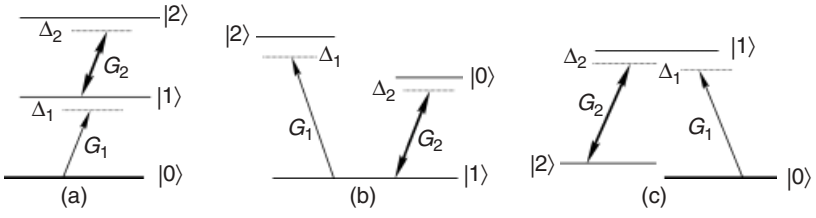

Figure 1.3 The diagrams of (a) a Ξ-type three-level, (b) a V-type three-level, and (c) a Λ-type three-level atomic systems, respectively.

interacting with a bright state, the bright state collapses into $|1\rangle$ and its corresponding eigenvalue is $\sqrt{G_1^2 + G_2^2}$. Thus, we can obtain the coefficients of the bright state as $C_0 = G_1 \exp(-i\Delta_1 t/\hbar)/\sqrt{G_1^2 + G_2^2}$, $C_2 = G_2 \exp(-i\Delta_2 t/\hbar)/\sqrt{G_1^2 + G_2^2}$, and $C_1 = 0$. Furthermore, as $|1\rangle$ and $|B\rangle$ are orthogonal with each other, the state of the system can be expanded into the linear combination of $|1\rangle$ and $|B\rangle$.

Next, when the coupled system is interacting with a dark state, the bright state turns into $|1\rangle$ and its corresponding eigenvalue is null. Therefore, with the equation of $H|\psi\rangle = 0$, we can easily get the coefficients in the expression of dark state as $C_0 = G_1 \exp(-i\Delta_1 t/\hbar)/\sqrt{G_1^2 + G_2^2}$, $C_2 = -G_2 \exp(-i\Delta_2 t/\hbar)/\sqrt{G_1^2 + G_2^2}$, and $C_1 = 0$.

From the expression of dark state, we can see that C_2 is leading to or lagging from C_0 by a π phase factor, so $|0\rangle$ and $|2\rangle$ can produce destructive interference and dark state resulting in EIT. However, in bright state, C_2 is in-phase with C_0; therefore, state $|0\rangle$ has constructive interference with state $|2\rangle$, which leads to electromagnetically induced absorption (EIA). Furthermore, by changing the dressing field's detuning and intensities, and the interaction times (phase), the bright and dark states can be controlled to evolve or, in other words, transform into each other.

In the above-mentioned switch between bright and dark states in ladder-type three-level systems, we have found that the FWM process also is significantly influenced. We have in experiment demonstrated the evolution of FWM, which is fitted well with the theoretical calculation based on the dark-state theory. Furthermore, more than one external dressing field is usually used, as shown in Figure 1.4, so more than one dark state emerges in such multi-level systems. In the following, we give a brief description on how multi-dark states can be obtained with state superposition theory.

When the dressing fields $\boldsymbol{E}_2$ and $\boldsymbol{E}_4$ are all strong sufficiently in Y-type four-level systems, their dressing effects on the FWM process will be affected by the quantum interference. We can obtain the Hamilton in the interaction picture,

$$\begin{aligned} \mathrm{H} = &-\hbar(\Delta_4|4\rangle\langle 4| + \Delta_2|2\rangle\langle 2| - \Delta_1|0\rangle\langle 0|) \\ &-\hbar(G_1|0\rangle\langle 1| + G_2|2\rangle\langle 1| + G_4|4\rangle\langle 1| + \mathrm{HC}) \end{aligned} \tag{1.1}$$

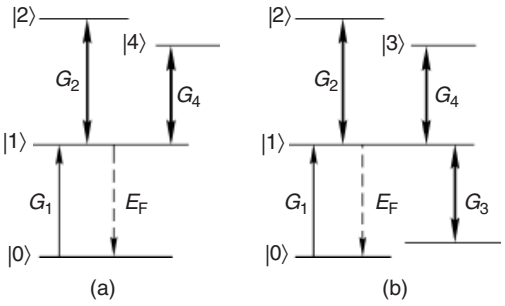

Figure 1.4 The diagrams of (a) a Y-type four-level and (b) a K-type five-level atomic systems.

Under the resonant conditions of $G_2, G_4 \gg G_1$, $\Delta_1 + \Delta_2 = 0$, and $\Delta_2 = 0$, we can get three independent dark states:

$$|D1\rangle = \frac{G_2|0\rangle - G_1|2\rangle}{\sqrt{|G_1|^2 + |G_2|^2}} \simeq |0\rangle - \frac{G_1}{G_2}|2\rangle \tag{1.2}$$

$$|D2\rangle = \frac{G_4|0\rangle - G_1|4\rangle}{\sqrt{|G_4|^2 + |G_1|^2}} \simeq |0\rangle - \frac{G_1}{G_4}|3\rangle \tag{1.3}$$

$$|D4\rangle = \frac{G_4|2\rangle - G_2|4\rangle}{\sqrt{|G_2|^2 + |G_4|^2}} = \cos\theta|2\rangle - \sin\theta|3\rangle \tag{1.4}$$

where $\cos\theta = G_4/\sqrt{|G_2|^2 + |G_4|^2}$ and $\sin\theta = G_2/\sqrt{|G_2|^2 + |G_4|^2}$. Therefore, the total dark-state amplitude is then given by

$$|D\rangle = |D1\rangle + |D2\rangle + |D4\rangle = 2|0\rangle + \left(\cos\theta - \frac{G_1}{G_2}\right)|2\rangle - \left(\frac{G_1}{G_4} + \sin\theta\right)|4\rangle \tag{1.5}$$

Utilizing the same calculation process, we can easily get the dark state in the K-type five-level atomic system:

$$|D'\rangle = 3|0\rangle - \frac{G_1}{G_2}|2\rangle - \left(\frac{G_1}{G_4} - \cos^*\theta\right)|4\rangle - \left(\frac{G_1}{G_3} + \sin^*\theta\right)|3\rangle \tag{1.6}$$

where $\cos^*\theta = G_3/\sqrt{|G_3|^2 + |G_4|^2}$ and $\sin^*\theta = G_4/\sqrt{|G_3|^2 + |G_4|^2}$.

On the other hand, in order to understand how the three independent dark states interfere with each other in Figure 1.4(a), we calculate the probability of an atom locating at dark state as

$$\begin{aligned}|\langle D|\varphi\rangle|^2 = {} & 4\rho_{00} + \left(\cos\theta - \frac{G_1}{G_2}\right)^2\rho_{22} + \left(\frac{G_1}{G_4} + \sin\theta\right)^2\rho_{44} \\ & + 4\mathrm{Re}\left(\left(\cos\theta - \frac{G_1}{G_2}\right)\rho_{20} - \left(\frac{G_1}{G_4} + \sin\theta\right)\rho_{40}\right) \\ & - 4\mathrm{Re}\left(\left(\frac{G_1}{G_4} + \sin\theta\right)\left(\cos\theta - \frac{G_1}{G_2}\right)^*\rho_{42}\right)\end{aligned} \tag{1.7}$$

where $|\varphi\rangle = c_0|0\rangle + c_1|1\rangle + c_2|2\rangle + c_3|4\rangle$ is the wave function of the atom in its bare-state basis; $\rho_{ii}(i = 1, 2, 3, 4)$ is the probability of the one atom populating in state $|i\rangle$; $\rho_{ij}(i, j = 1, 2, 3, 4)$ is proportional to the dipole moment between $|i\rangle$ and $|j\rangle$. Among them, the populations are assumed to be $\rho_{00} \approx 1$, $\rho_{22} \approx 0$, and $\rho_{44} \approx 0$ in Eq. (1.5). By exploring the quantum interference among the three states $|0\rangle$, $|2\rangle$, and $|4\rangle$, the intensity of the FWM signal is obtained as $I = |N'\mu\rho_{10}^{(3)}|^2$, where $N' = N(1 - |\langle D|\psi\rangle|^2)$ is the weight factor describing the number density of atoms not in dark states, with N being the total particle number density. Therefore, it is obvious that the quantum interference effect can exert an influence on the FWM signals via changing the effective number density particle participating in the FWM process.

As only the dark states $|D2\rangle$ and $|D4\rangle$ are related to the field $\boldsymbol{E}_4$, with G_4 increasing, both the probability amplitudes of the states $|D2\rangle$ and $|D4\rangle$ will grow and the theoretical result of $|\langle D2|\psi\rangle|^2 > |\langle D4|\psi\rangle|^2$ means that the probability amplitude of state $|D2\rangle$ is stronger than that of $|D4\rangle$. So the controls of the two dark states will bring different results in the FWM processes.

1.1.3
Suppression and Enhancement Conditions

In the previous section, we have discussed singly- and doubly-dressed MWM process in a multi-level atomic system by scanning the detuning of the dressing field [32, 33]. However, the interactions between the dressed states are not involved. In this section, with such an interaction introduced, not only three kinds of doubly-dressed schemes (nested-, parallel-, and sequential-cascade modes) of MWMs are analyzed and discussed in depth but the transition between the bright and dark states is also given.

As shown in Figure 1.5, the fields $\boldsymbol{E}_3$ (Figure 1.5(a)) and $\boldsymbol{E}_2$ (Figure 1.5(b)) dress the energy level $|1\rangle$ to form a Λ-type or Ξ-type singly-dressed system via the perturbation subchains $\rho_{10} \xrightarrow{-\omega_3} \rho_{30} \xrightarrow{\omega_3} \rho_{10}$ and $\rho_{10} \xrightarrow{\omega_2} \rho_{20} \xrightarrow{-\omega_2} \rho_{10}$, respectively. Therefore, we get the evolution of a singly-dressed FWM and its corresponding probe transmission signal shown in Figure 1.6. Comparing the two dressed systems, we can see that the transition sequence is almost opposite, which can be explained using the dark-state theory. With $\Delta_1 < 0$, the signals are resonant with the left dark state and right bright state in Λ-type singly-dressed case (Figure 1.6(a); however, the distribution order of dark and bright state is reverse in the Ξ-type level structure as shown in Figure 1.6(b). One symmetric center at $\Delta_1 = 0$ is observed in such cases.

Next, we introduce the doubly-dressed effect on the generation process of FWM and probe transmission signals. It is generally divided into parallel-, nested-, and sequential-cascade modes. First, in the parallel-type doubly-dressed case, as shown in Figure 1.7(a), the fields $\boldsymbol{E}_3$ and $\boldsymbol{E}_4$ dress different level $|1\rangle$ and $|0\rangle$, via the subchains $\rho_{10} \xrightarrow{-\omega_3} \rho_{30} \xrightarrow{\omega_3} \rho_{10}$ $(\rho_{(G_3\pm)0})$ and $\rho_{20} \xrightarrow{-\omega_4} \rho_{24} \xrightarrow{\omega_4} \rho_{20}$ $(\rho_{2(G_4\pm)})$, respectively. This means that the dressing effects of $\boldsymbol{E}_3$ and $\boldsymbol{E}_4$ lie parallel. In the parallel-cascade case, the profiles (dashed lines in Figure 1.8(a)) are induced by one

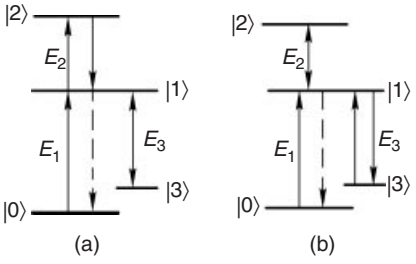

Figure 1.5 (a) Λ- and (b) Ξ-type singly-dressed FWM.

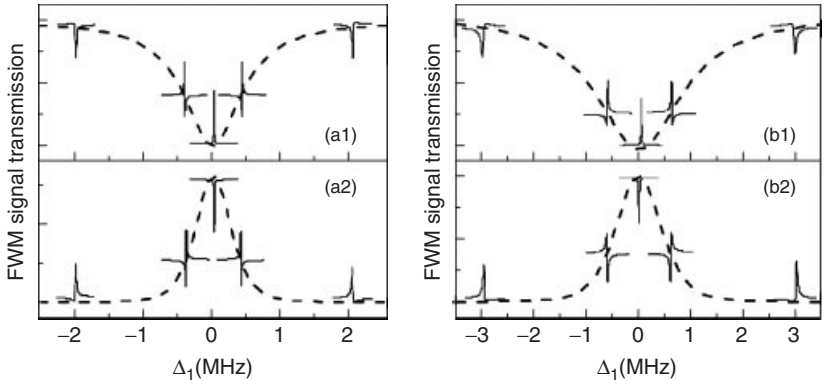

Figure 1.6 (a1) and (b1) Singly-dressed Λ-type and Ξ-type probe transmission signals. (a2) and (b2) the corresponding FWM signals. The dashed curves in (a) and (b) are the probe transmission and the corresponding pure FWM signals without $\boldsymbol{E}_3$ or $\boldsymbol{E}_2$, respectively.

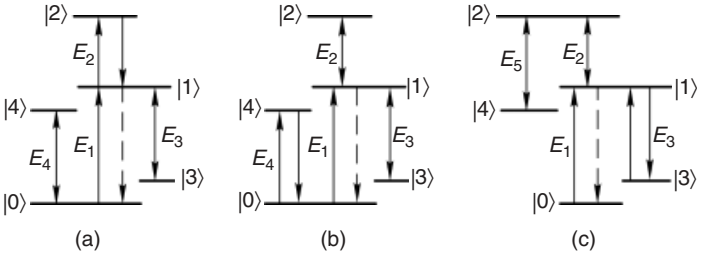

Figure 1.7 (a) Parallel-cascade, (b) sequential-cascade, and (c) nested-cascade mode doubly-dressed FWMs, respectively.

dressing field, and the transition between bright and dark states (in Figure 1.8(a)) is caused by the other dressing field. So, the two dressing fields in the parallel-dressed cascade mode have no interaction. Only one symmetric center at $\Delta_1 = 0$ is observed in such cases too.

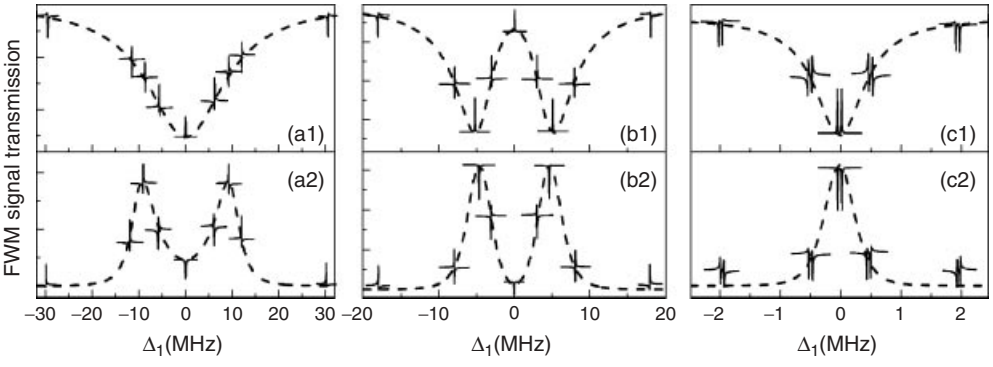

Figure 1.8 (a1), (b1), and (c1) Parallel-cascade, sequential-cascade, and nested-cascade doubly-dressed probe transmission signal, respectively. (a2), (b2), and (c2) the corresponding FWM signal. The dashed curves in (a), (b), and (c) are the probe transmission and the corresponding pure FWM signals without $\boldsymbol{E}_3$ or $\boldsymbol{E}_5$, respectively.

In Figure 1.7(b), the FWM signal is in sequential-cascade doubly-dressed mode (dressed by $\boldsymbol{E}_2$ and $\boldsymbol{E}_3$), in which the fields $\boldsymbol{E}_2$ and $\boldsymbol{E}_3$ dress the same level $|1\rangle$ via the subchain $\rho_{10} \xrightarrow{\omega_2} \rho_{20} \xrightarrow{-\omega_2} \rho_{10} \xrightarrow{-\omega_3} \rho_{30} \xrightarrow{\omega_3} \rho_{10}$. This means that the dressing effects of $\boldsymbol{E}_2$ ($\rho_{10} \xrightarrow{\omega_2} \rho_{20} \xrightarrow{-\omega_2} \rho_{10}$) and $\boldsymbol{E}_3$ ($\rho_{10} \xrightarrow{-\omega_3} \rho_{30} \xrightarrow{\omega_3} \rho_{10}$) join together sequentially; therefore, we call this type of dressing mode as sequential-cascade mode. The profiles of the FWM (i.e., AT splitting) and probe transmission (i.e., EIT) (the dashed lines in Figure 1.8(b)) show the double-peak and double-dip structure versus Δ_1 with $\boldsymbol{E}_2$ blocked. The transition between bright and dark states (in Figure 1.8(b)) is caused by $\boldsymbol{E}_2$. Both the signals in Figure 1.8(b) show three symmetric centers that reflect the interaction between two dressing fields. In the comparison between the sequential-cascade mode and parallel-cascade mode, the transition between the bright and dark states reveals interaction between the two dressing fields in the former mode, while no interaction is revealed in the latter mode.

In Figure 1.7(c), the FWM signal is in the nested doubly-dressed mode (inner-dressing field $\boldsymbol{E}_2$ and outer-dressing field $\boldsymbol{E}_5$), in which $\boldsymbol{E}_5$ dresses the same level $|1\rangle$ after the inner-dressing field $\boldsymbol{E}_2$ having dressed it. This means the dressing effect of $\boldsymbol{E}_5$ ($\rho_{20} \xrightarrow{-\omega_5} \rho_{40} \xrightarrow{\omega_5} \rho_{20}$) is nested in that of $\boldsymbol{E}_2$ ($\rho_{10} \xrightarrow{\omega_2} \rho_{20}$ and $\rho_{20} \xrightarrow{-\omega_2} \rho_{10}$). By scanning the detuning of the inner-dressing field $\boldsymbol{E}_2$, the dashed lines in Figure 1.8(c) show one AT splitting structure in the pure FWM signal and EIT window in probe transmission signal. In such cases, there is only one symmetric center when the inner-dressing field is scanned, but three symmetric centers when the outer-dressing field is scanned, as reflects the strong interaction between two dressing fields. In comparison between the nested-cascade and sequential-cascade dressing modes, the interaction between the two dressing fields in the former mode is stronger, and reflected as dual bright state and dual dark state in the evolution of the FWM signal and probe transmission.

1.2 Fluorescence in MWM

Traditional fluorescence is defined as emitted light by an object, which usually has a longer wavelength than the absorbed radiation. However, in case those two photons are absorbed by one atom, the emission with shorter wavelength than the photon absorbed can be obtained. Furthermore, the emitted field may also be of the same wavelength as the absorbed radiation, termed *resonance fluorescence*.

This section provides a brief description of the two-photon fluorescence process that accompanies the MWM process. In our theoretical and experimental scheme, both MWM signals and fluorescence signals are transmitted in an EIT window. Therefore, compared with resonance fluorescence, the fluorescence process with MWM has several distinct differences and advantages. First, extremely narrow fluorescence signals (about 50 MHz) can be obtained in an open-cycle atomic system, as the generated fluorescence signals fall into EIT windows. Such fluorescence signals with extremely narrow line widths have not been reported before, either experimentally or theoretically. This will allow us to investigate the quantum correlation and narrow line width laser as the generated fluorescence signal is very high in coherence and monochromaticity. Second, by individually controlling the EIT windows, fluorescence signals can be clearly separated or superimposed selectively. Third, the amplitude of the fluorescence signal can be controlled by changing the intensity and frequency of pumping laser via dark states.

In order to give a clear physical description of the fluorescence process, we consider six types of level structures, two-level, V-, Λ-, and Ξ-type three-level, Y- and reversed Y-type four-level atomic systems, as shown in Figure 1.9. First, for the two-level system (Figure 1.9(a)), the single- and two-photon fluorescence signals R_1 and R_2 will be generated as a result of the spontaneous emission of photons from $|1\rangle$ to $|0\rangle$, which can be described by the Liouville pathways $(R_1)\ \rho_{00}^{(0)} \xrightarrow{\omega_1} \rho_{10}^{(1)} \xrightarrow{-\omega_1} \rho_{11}^{(2)}$ and $(R_2)\ \rho_{00}^{(0)} \xrightarrow{\omega_1} \rho_{10}^{(1)} \xrightarrow{-\omega_2} \rho_{00}^{(2)} \xrightarrow{\omega_2} \rho_{10}^{(3)} \xrightarrow{-\omega_1} \rho_{11}^{(4)}$, respectively. Next, for the V-type three-level system (Figure 1.9(b)), there exist two single-photon fluorescence signals R_1 (from $|1\rangle$ to $|0\rangle$) and R_2 (from $|2\rangle$ to $|0\rangle$), and two two-photon fluorescence signals R_3 (from $|1\rangle$ to $|0\rangle$) and R_4 (from $|2\rangle$ to $|0\rangle$), which can be described by the Liouville pathways $(R_1)\ \rho_{00}^{(0)} \xrightarrow{\omega_1} \rho_{10}^{(1)} \xrightarrow{-\omega_1} \rho_{11}^{(2)}$, $(R_2)\ \rho_{00}^{(0)} \xrightarrow{\omega_2} \rho_{20}^{(1)} \xrightarrow{-\omega_2} \rho_{22}^{(2)}$, $(R_3)\ \rho_{00}^{(0)} \xrightarrow{\omega_1} \rho_{10}^{(1)} \xrightarrow{-\omega_2} \rho_{12}^{(2)} \xrightarrow{\omega_2} \rho_{10}^{(3)} \xrightarrow{-\omega_1} \rho_{11}^{(4)}$, and $(R_4)\ \rho_{00}^{(0)} \xrightarrow{\omega_2} \rho_{20}^{(1)} \xrightarrow{-\omega_1} \rho_{21}^{(2)} \xrightarrow{\omega_1} \rho_{20}^{(3)} \xrightarrow{-\omega_2} \rho_{22}^{(4)}$. Then, for the Λ-type system three-level (Figure 1.9(c)), the decay of photons from $|1\rangle$ to $|0\rangle$ will generate single- and two-photon fluorescence signals R_1 and R_2, which can be described via the Liouville pathways $(R_1)\ \rho_{00}^{(0)} \xrightarrow{\omega_1} \rho_{10}^{(1)} \xrightarrow{-\omega_1} \rho_{11}^{(2)}$ and $(R_2)\ \rho_{00}^{(0)} \xrightarrow{\omega_1} \rho_{10}^{(1)} \xrightarrow{-\omega_2} \rho_{20}^{(2)} \xrightarrow{\omega_2} \rho_{10}^{(3)} \xrightarrow{-\omega_1} \rho_{11}^{(4)}$, respectively. While for the Ξ-type system (Figure 1.9(d)), there is only one single-photon fluorescence signal R_1 and one two-photon signal R_2, which can be represented by the Liouville pathways $(R_1)\ \rho_{00}^{(0)} \xrightarrow{\omega_1} \rho_{10}^{(1)} \xrightarrow{-\omega_1} \rho_{11}^{(2)}$ (spontaneous emission from $|1\rangle$ to $|0\rangle$) and $(R_2)\ \rho_{00}^{(0)} \xrightarrow{\omega_1} \rho_{10}^{(1)} \xrightarrow{\omega_2} \rho_{20}^{(2)} \xrightarrow{-\omega_1} \rho_{21}^{(3)} \xrightarrow{-\omega_2} \rho_{22}^{(4)}$ (spontaneous emission from $|2\rangle$ to $|1\rangle$), respectively. Further, for the Y-type four-level system (Figure 1.9 (e)), there is an additional two-photon fluorescence signal R_3

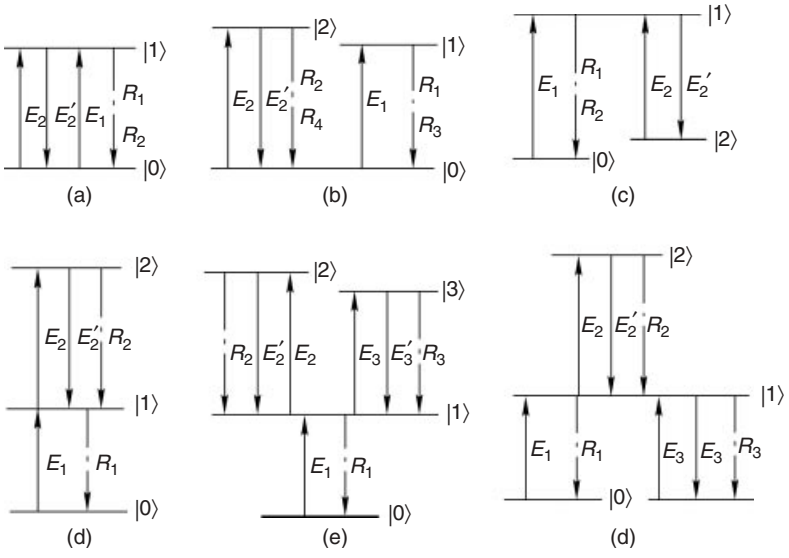

Figure 1.9 The diagrams of (a) two-level, (b) a three-level V-type, (c) a three-level Λ-type, (d) a three-level Ξ-type, and (e) four-level Y-type atomic systems.

compared to the three-level Ξ-type system (Figure 1.9 (d)), which is the spontaneous emission from $|3\rangle$ to $|1\rangle$, and can be expressed by the Liouville pathway (R_3) $\rho_{00}^{(0)} \xrightarrow{\omega_1} \rho_{10}^{(1)} \xrightarrow{\omega_3} \rho_{30}^{(2)} \xrightarrow{-\omega_1} \rho_{31}^{(3)} \xrightarrow{-\omega_3} \rho_{33}^{(4)}$. Here, we only give the corresponding doubly-dressed density matrix elements for the Y-type four-level system as follows:

$$\rho_{11}^{(2)} = \frac{-|G_1|^2}{\Gamma_{11}(d_1 + |G_2|^2/d_2 + |G_3|^2/d_3)} \tag{1.8}$$

$$\rho_{22}^{(4)} = \frac{|G_1|^2|G_2|^2}{\Gamma_{22}d_1d_4(d_2 + |G_2|^2/(d_1 + |G_3|^2/d_3))} \tag{1.9}$$

$$\rho_{33}^{(4)} = \frac{|G_1|^2|G_3|^2}{\Gamma_{33}d_1d_5(d_3 + |G_3|^2/(d_1 + |G_2|^2/d_2))} \tag{1.10}$$

where $d_1 = \Gamma_{10} + i\Delta_1$, $d_2 = \Gamma_{20} + i(\Delta_1 + \Delta_2)$, $d_3 = \Gamma_{30} + i(\Delta_1 + \Delta_3)$, $d_4 = \Gamma_{21} + i\Delta_2$, and $d_5 = \Gamma_{31} + i\Delta_3$ with frequency detuning $\Delta_i = \Omega_i - \omega_i$ (Ω_i is the resonance frequency of the transition driven by E_i) and transverse relaxation rate Γ_{ij} between $|i\rangle$ and $|j\rangle$. Finally, the reversed Y-type four-level system (Figure 1.9(f)), will also generate an additional two-photon fluorescence signal R_3, compared with the Ξ-type system, which can be presented as (R_3) $\rho_{00}^{(0)} \xrightarrow{\omega_1} \rho_{10}^{(1)} \xrightarrow{-\omega_3} \rho_{30}^{(2)} \xrightarrow{\omega_3} \rho_{10}^{(3)} \xrightarrow{-\omega_1} \rho_{11}^{(4)}$ (spontaneous emission from $|1\rangle$ to $|0\rangle$).

By scanning Δ_1, the probe transmission, FWM and fluorescence signals (Figure 1.10(a)) in the Y-type system are obtained. In the fluorescence signals, the global background represents the single-photon fluorescence R_1 ($\rho_{11}^{(2)}$), and other two small sharp peaks on it are derived from the two-photon fluorescence

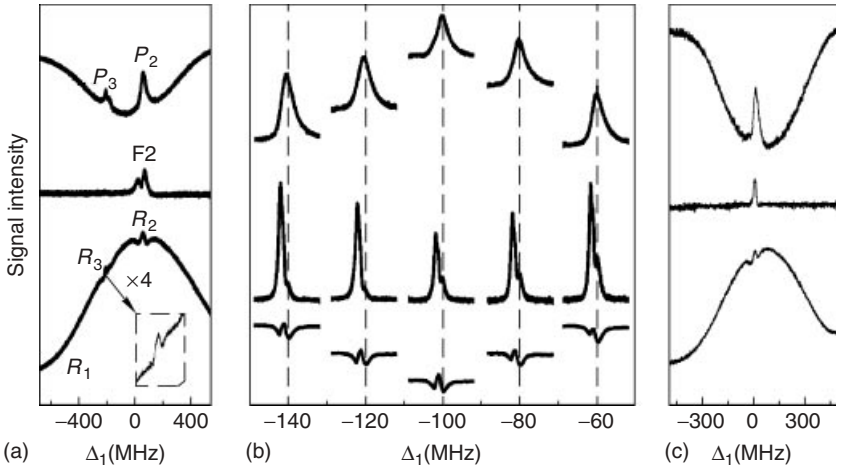

Figure 1.10 Measured probe transmission (upper curves), MWM (middle curves), and fluorescence (bottom curves) ((a) and (c)) versus probe detuning Δ_1, (b) versus Δ_2 at discrete Δ_1 in Y-type ((a) and (b)) and inverted Y-type (c) four-level atomic system.

signals R_2 ($\rho_{22}^{(4)}$) and R_3 ($\rho_{33}^{(4)}$). Figure 1.10(b) represents the measured signals by scanning Δ_2 at discrete Δ_1. Similarly, for the fluorescence signal, the global profile expresses the dressed R_1 ($\rho_{11}^{(2)}$) by E_3; the dip lower than the corresponding baseline represents further dressed R_1 ($\rho_{11}^{(2)}$) by E_2, and the peak within the dip is the two-photon fluorescence signal R_2 ($\rho_{22}^{(4)}$). Furthermore, Figure 1.10(c) represents the probe transmission, SWM, and fluorescence versus Δ_1 in the reversed Y-type system. Similarly, the global background represents the fluorescence R_1 and R_3 ($\rho_{11}^{(2)}$ and $\rho_{11}^{(4)}$), and the small sharp peak on it is the two-photon fluorescence R_2 ($\rho_{22}^{(4)}$).

Although generated simultaneously, the two-photon fluorescence signal and the FWM signals have different behaviors and the difference can be seen from the Liouville pathway. First, the FWM signal is caused by the atomic coherence effect, while the fluorescence signal is induced by spontaneous decay of photons pumped to the upper levels. Second, the direction of the FWM signal is determined by the limitations of the phase-matching conditions, but the fluorescence signal is not directional. Third, the FWM process follows the closed-loop path while the fluorescence process does not.

1.3 MWM Process in Ring Optical Cavity

In this section, we consider the MWM process in the ring cavity. First, a brief discussion on the relation between atom-cavity coupling strength and cavity mode splitting, and how the intensities of input and output are affected by atom-cavity coupling strength are given. Next, noise squeezing with nonlinear media in ring

cavity is studied. As an important entanglement light source, squeezed light field with FWM process is briefly discussed.

1.3.1
High-Order Cavity Mode Splitting with MWM Process

VRS has been reported when single two-level atom or N two-level atoms are strongly coupled with cavity mode. The frequency separation of the VRS are $2g$ and $2G$ in the two atom-cavity systems, respectively, with g and $G = g\sqrt{N}$ being single- and multi-atom coupling strength, respectively. The coherently prepared atom-cavity system will also result in the intracavity EIT results, OB, and multi-stability behavior, in which close contact between VRS and OB behavior can be deduced.

In this section, we investigate the relationship between the VRS and OB of the generated MWM cavity mode, achieve the control of VRS and OB simultaneously by the coherent control of dark and bright states, and get the inclined VRS.

As shown in Figure 1.11, the coupled atom-cavity system consisting of Rubidium atoms confined in a four-mirror-formed ring cavity, in which only the generated FWM (SWM) signal can form the cavity mode. Figure 1.12 gives the transmission spectra of the FWM (E_1, E_2, E_2') cavity mode, containing the splitting positions and heights of the multi-modes. For an empty cavity, the cavity transmission spectra has Lorentzian shape and equal mode spacing (free spectral range Δ_{FSR}), shown as the dashed curves in Figure 1.12. For the coupled atom-cavity system, not only is the zero-order longitudinal mode split with symmetrical center $\Delta_1 = 0$ (Figure 1.12(a1)) but high-order modes are also split by the cavity field when the coupling strength $g\sqrt{N}$ is increased to near or larger than Δ_{FSR}, shown as the solid curves in Figure 1.12(a2) to (a4).

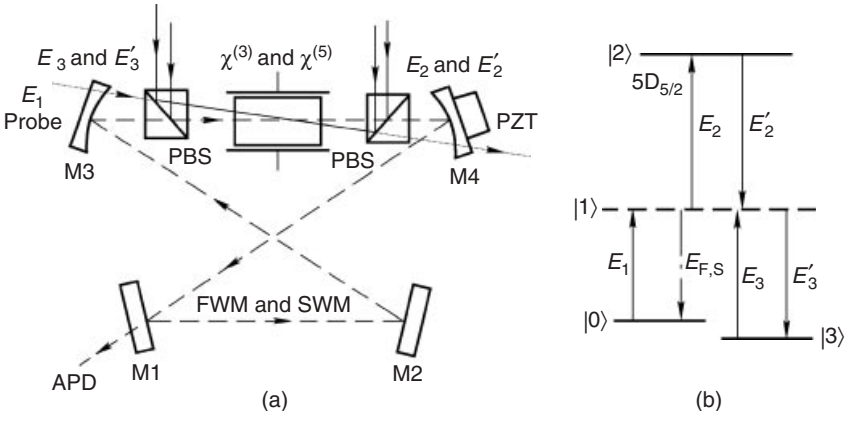

Figure 1.11 (a) A scheme of a ring cavity containing the four-level atoms to generate FWM and SWM processes. (b) Scheme of the four-level atomic system.

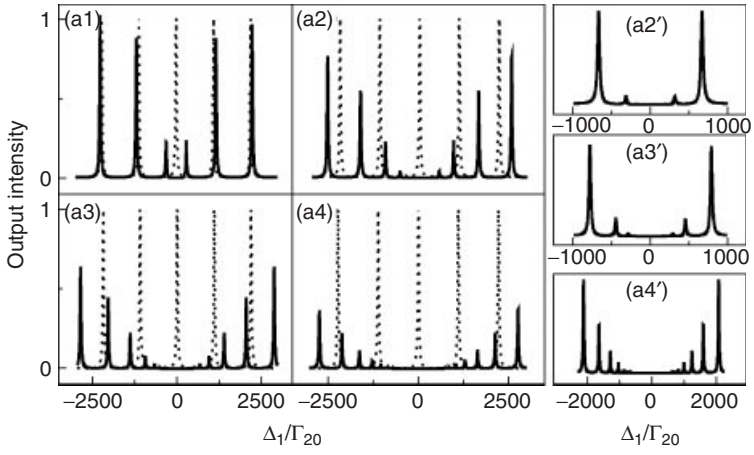

Figure 1.12 (a1)–(a4) Solid curves are transmission spectra of the generated FWM cavity mode with N increasing. Dashed curves are the transmission spectra of empty cavity. The illustrations (a2′)–(a4′) FWM cavity mode transmissions in smaller regions corresponding to (a2)–(a4).

Next, the relationship between the input–output intensities under steady-state condition is shown in Figure 1.13, which displays OB behavior of the transmitted FWM cavity mode influenced by dark state. In detail, Figure 1.13(a) illustrates the output intensity of the FWM cavity mode versus probe input intensity (I_i) and detuning (Δ_1), which represents the modulation of VRS in frequency domain and input–output relationship (OB behavior) simultaneously. With I_i increasing, the spectrum of the transmitted FWM cavity mode expands rapidly when Δ_1 is scanned, as shown in Figure 1.13(b). Figure 1.13(c) obviously shows OB hysteresis cycle and the threshold of the optical parametric amplification (OPA) FWM process, and reveals that the increasing $|\Delta_1|$ can result in a significant change in the OB behavior with the increase in the right OB threshold value. Finally, Figure 1.13(d) displays the OB threshold values at different Δ_1, in which the left OB threshold value shifts slowly while the right one shifts sharply. Moreover, Figure 1.13(d) directly predicts there is no OB at or close to the position of dark state ($\Delta_1/\Gamma_{20} = 0$), which results from disappearing linear dispersion at $\Delta_1/\Gamma_{20} = 0$ by the interference between two possible absorption channels $|0\rangle \rightarrow |\pm\rangle$ induced by g^2N.

1.3.2
Squeezed Noise Power with MWM

The quantum correlations have been presented in signal and idler lights from type I and type II [34, 35] OPA inside an optical cavity, which have recently generated increased interests. Moreover, the FWM or SWM processes, which are assisted by the EIT window in multi-level atomic systems, are efficient sources for squeezed radiation and correlated photons. Recent experiments have demonstrated the slowing down [36–38], storage, and retrieval [39, 40] of squeezed states of light